# Towards high selectivity aniline synthesis catalysis at elevated temperatures

Clément G.A. Morisse [1], Annelouise M. McCullagh [1], James W. Campbell [1], Colin How [2], Donald A. MacLaren [2], Robert H. Carr [3], Chris J. Mitchell [4] and David Lennon [1*]

1. School of Chemistry, Joseph Black Building, University of Glasgow, Glasgow, G12 8QQ, UK.
2. School of Physics and Astronomy, Kelvin Building, University of Glasgow, Glasgow, G12 8QQ, UK.
3. Huntsman Polyurethanes, Everslaan 45, 3078 Everberg, Belgium.
4. SABIC UK Petrochemicals Ltd., The Wilton Centre, Redcar, TS10 4RF, UK.

*Email: David.Lennon@glasgow.ac.uk
Telephone: +44-141-330-4372

**Abstract**

In connection with an initiative to enhance heat recovery from the large-scale operation of a heterogeneously catalysed nitrobenzene hydrogenation process to produce aniline, it is necessary to operate the process at elevated temperatures (>100°C), a condition that can compromise aniline selectivity. Alumina-supported palladium catalysts are selected as candidate materials that can provide sustained aniline yields at elevated temperatures. Two $Pd/Al_2O_3$ catalysts are examined that possess comparable mean Pd particle sizes (~5 nm) for different Pd loading: 5 wt % $Pd/Al_2O_3$ and 0.3 wt % $Pd/Al_2O_3$. The higher Pd loading sample represents a reference catalyst for which the Pd crystallite morphology has previously been established. The lower Pd loading technical catalyst more closely corresponds to industrial specifications. The morphology of the Pd crystallites of the 0.3 wt % $Pd/Al_2O_3$ sample is explored by means of temperature-programmed infrared spectroscopy of chemisorbed CO. Reaction testing over the range 60-180°C shows effectively complete nitrobenzene conversion for both catalysts but with distinction in their selectivity profiles. With reference to a reaction scheme, the low loading catalyst is favoured as it maximises aniline selectivity and avoids the formation of over-hydrogenated products. A plot of aniline yield as a function of WHSV for the 0.3 wt % $Pd/Al_2O_3$ catalyst at 100°C yields a 'volcano' like curve, indicating aniline selectivity to be sensitive to residence time. These observations are brought together to provide an indication of an aniline synthesis catalyst specification suited to a unit operation equipped for enhanced heat transfer.

**Keywords**

Nitrobenzene hydrogenation; $Pd/Al_2O_3$ catalysts; aniline synthesis, by-product formation; metal crystallite morphology.

## 1. Introduction

Polyurethanes are classed as speciality polymers that find wide application in modern society. For example, they are used in fields as diverse as furnishings, the construction sector, insulation, and as components used in aircrafts and cars. Polyurethanes are prepared by the reaction between isocyanates and polyols. More than 90% of polyurethanes are produced from aromatic poly-isocyanates, with toluene diisocyanate (TDI) and methylene diphenyl diisocyanate (MDI) being the dominant materials [1]. Over recent years the polyurethane industry has exhibited annual growth rates of 4-5%, with annual consumption in 2017 reported to exceed 20 Mt. This growth is expected to continue for the foreseeable future [1]. MDI is produced via the condensation of aniline with formaldehyde in the presence of an acid (*e.g.*, HCl) [2]. Thus, aniline is a major component of any large-scale isocyanate production chain, where it is usually produced by the heterogeneously catalysed hydrogenation of nitrobenzene (Scheme 1). Kahl and co-workers have reviewed the catalyst and process options applied to large-scale aniline production, with reactions typically performed at full nitrobenzene conversion [3]. It is estimated that in 2008 approximately 3.0 Mt of aniline were consumed in the production of isocyanates, mainly MDI [3].

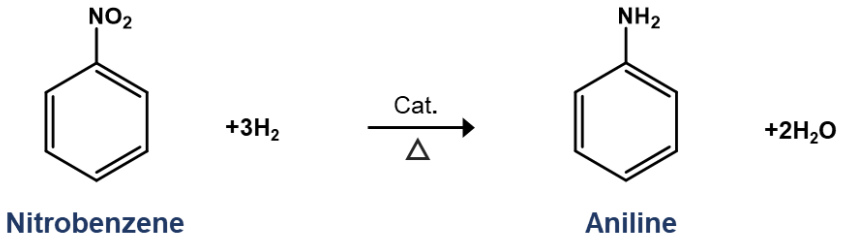


Scheme 1. The hydrogenation of nitrobenzene to produce aniline.

Due to the complexity of the MDI manufacturing process, not least due to the involvement of phosgene as a reagent, isocyanate production is normally undertaken within an integrated chemicals complex [4]. In recent years, there has been an increasing intention to minimise energy costs and to improve overall operational efficiency of such facilities. One route to achieve these goals is to ensure efficient heat recovery from highly exothermic reactions.

The formation of steam in heat recovery processes is common [5], [6], [7], [8] and is achieved via the vaporisation of water at 100°C for standard pressures. Heating of steam exceeding its boiling point for a given pressure results in the formation of "dry steam", or as it is otherwise known super-heated steam [9]. Super-heated steam is higher in energy than that of saturated steam – an energy increase of 30 kJ $kg^{-1}$ is reported when comparing saturated steam (100°C, 1 barg) to superheated steam (110°C) [10]. This highlights the considerable energy output which may be harnessed by operating reactors

at elevated temperatures to produce super-heated steam which subsequently can be utilised for further chemical processes or, alternatively, to generate electricity [11]. Within the context of an isocyanate production facility, the hydrogenation of nitrobenzene, which exhibits standard reaction enthalpies of -554.1 and -468.2 kJ $mol^{-1}$ for the liquid and vapour phases respectively [12], is ideally suited to raise super-heated steam. However, this would require running the reaction at elevated temperatures (≥ 100°C), a condition that can compromise catalytic selectivity.

Nitrobenzene hydrogenation with high aniline selectivity is achievable with a plethora of different metal supported catalysts including palladium [13], [14], nickel [15], platinum [16] and copper [17]. Pd based catalysts exhibit high activity and preferential reduction of functional groups in proximity to aromatic systems, and so are widely reported in literature for nitrobenzene hydrogenation at high aniline selectivity[18], [19], [20]. Pd supported on alumina is suited to the higher temperature operational platform connected with heat recovery options relevant to large-scale aniline production facilities.

Sá Couto et al. have reported on outcomes linked to liquid phase nitrobenzene hydrogenation over a series of $Pd/Al_2O_3$ catalysts. Specifically, a parametric investigation of nitrobenzene hydrogenation with a 1 wt % $Pd/Al_2O_3$ catalyst in a 3-phase basket reactor revealed increasing temperature as the parameter which primarily influenced the production of secondary by-products, more so than was observed for increasing pressure (14 – 30 barg) or initial nitrobenzene concentration (3 – 10 wt % NB) [21]. Benzene was isolated as a by-product of nitrobenzene hydrogenation and proposed to emerge from hydro-denitrogenation of aniline [21] (Scheme 2). It is noted however that the scheme presented by Sá Couto et al. does not address the formation of azobenzene, azoxybenzene or hydrazobenzene as observed by, for example, Gelder et al. [14].

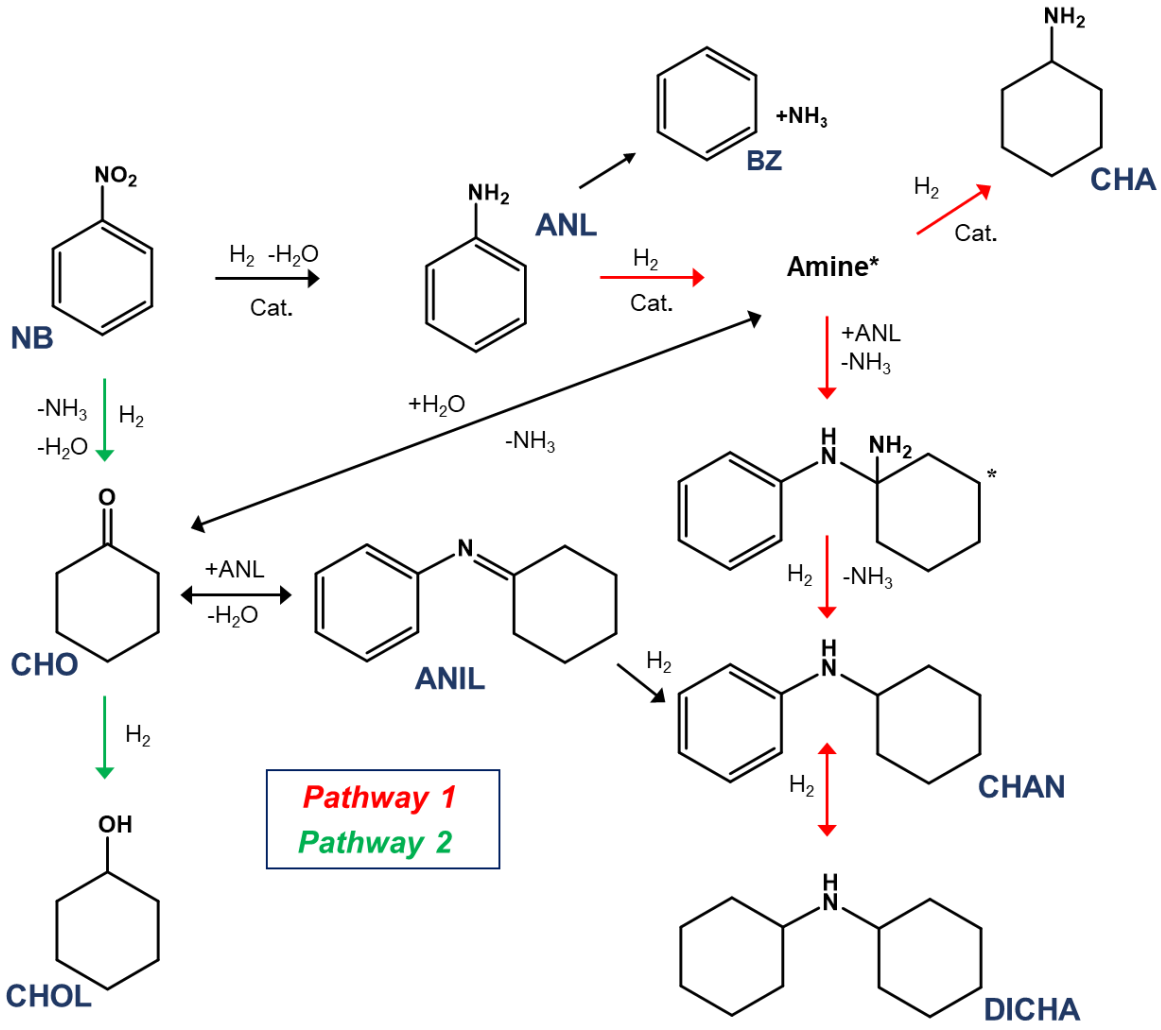


Scheme 2. Reaction scheme for nitrobenzene (NB) hydrogenation to aniline (ANL). Pathway 1 (products: cyclohexylamine (CHA), N-cyclohexylaniline (CHAN), dicyclohexylamine (DICHA)) is highlighted in red, whilst Pathway 2 (products: cyclohexanone (CHO) and cyclohexanol (CHOL)) is highlighted in green. The scheme is adapted from the work of Sá Couto et al. with permission of the original publisher [21].

Clearly, Scheme 2 shows the hydrogenation of nitrobenzene over $Pd/Al_2O_3$ to be a more complicated process than that implied by Scheme 1, with several pathways accessible that can compromise aniline selectivity. The first pathway, and most prominent, occurs from direct over-hydrogenation of aniline resulting in the production of cyclohexylamine (CHA), N-cyclohexylaniline (CHAN) and dicyclohexylamine (DICHA) (Scheme 2, red), with DICHA being the final hydrogenation product [21]. A second pathway (Scheme 2, green) is associated with the direct transformation of nitrobenzene to cyclohexanone (CHO), which can then be further hydrogenated to cyclohexanol (CHOL). Further work by Sá Couto et al. considered the effect of varying operational parameters on catalytic activity for

different Pd loadings and particle diameters [22]. More recently, Sá Couto et al. reported an increase in aniline selectivity with increasing time on stream using a 0.3 wt % $Pd/Al_2O_3$ catalyst in a trickle bed reactor, which is attributed to the blocking of active sites via carbon deposition that hinders production of heavy by-products (ANIL {N-Cyclohexylideneaniline }, CHAN, DICHA) [23].

The matter of morphological effects of supported Pd catalysts applied to selective hydrogenation reactions is a well-established concept [24], [25], [26]. This article builds on the previous studies but works towards more precisely defining the surface chemistry connected with sustained aniline production. Specifically, by-product formation of a particular catalyst formulation needs to be definitively established to guide the selection of a suitable post-reaction purification stage (*i.e.*, distillation unit) for any intended plant revisions at the industrial complex [27], [28]. To this end, two $Pd/Al_2O_3$ catalysts are examined: a 5 wt % $Pd/Al_2O_3$ catalyst and a 0.3 wt % $Pd/Al_2O_3$ technical grade catalyst. The former represents a reference catalyst, where the morphology of the Pd crystallites has been previously examined by diffuse reflectance infrared Fourier transform spectroscopy (DRIFTS) [29]. In contrast, the lower loading sample is potentially more suited to industrial application on cost grounds; its catalytic performance and morphological attributes will be compared to the reference material. Although a reduced Pd loading has economic benefits, the lower metal loading may result in a mass-transfer limited regime [30], [31]. To overcome this issue, the 0.3 wt % $Pd/Al_2O_3$ catalyst has been prepared to possess an 'egg-shell' distribution of Pd, where a thin shell of Pd is concentrated near the edge of the catalyst pellets [31], [32]. Importantly, the two catalysts exhibit comparable Pd particle sizes, thereby enabling particle size independent morphology deductions to be made that can be directly linked to a propensity for by-product formation. The article is constructed as follows. Both catalysts are comprehensively characterised, with the morphology of the low loading sample evaluated by application of CO chemisorption coupled with temperature-programmed infrared spectroscopy, a common method for determination of adsorption sites [33]. IR measurements of chemisorbed CO on low metal loading catalysts presents significant sensitivity issues arising from the reduced Pd content, thus the development of a method to permit collection of decipherable and meaningful IR spectra for chemisorbed CO on the 0.3 wt % $Pd/Al_2O_3$ catalyst is described. Reaction testing is performed in the vapour phase to facilitate post-reaction analysis. Reaction profiles over the temperature range 60-180°C performed in the presence of excess hydrogen show both samples to display high nitrobenzene conversions but distinct selectivity profiles. Concentrating on the lower Pd loading sample, aniline yield is shown to be sensitive to residence time. The results are discussed in terms of Pd morphology and operating conditions that minimise over-hydrogenation reactions.

Overall, the study makes a connection between by-product formation and catalyst specification that includes an awareness of Pd crystallite morphology.

## 2. Experimental

Two catalysts were used in this study: a 5 wt % $Pd/Al_2O_3$ sample (powder) obtained from Alfa Aesar (ref: 11713) and a 0.3 wt % $Pd/Al_2O_3$ technical egg-shell catalyst (pellets) that was supplied by Huntsman Polyurethanes (Ref: ASC-1). Henceforth, the 5 wt % catalyst will be referred to as GU-1 and the 0.3 wt % catalyst as GU-2.

### *2.1. Catalyst characterisation*

Palladium loading was measured by atomic absorption spectrophotometry (AAS) by means of a Perkin Elmer Analyst 100 instrument (λ = 244.8 nm) that was calibrated from a 1 g $L^{-1}$ Pd/HCl commercial stock solution (Sigma Aldrich). Samples were prepared for analysis by dissolving the catalyst sample (0.1 g) in aqua regia and boiling for 30 mins with fumes allowed to evaporate. After cooling, deionised water (5 mL) was added and the solution filtered into a 25 mL volumetric flask prior to measurement. Brunner-Emmett-Teller (BET) total surface area measurements were carried out on a Micromeritics ASAP 2400 gas adsorption analyser using a static barometric method. Catalyst samples (0.5 g) were placed into a glass tube and outgassed at 140 °C over-night in flowing nitrogen. Adsorption of nitrogen was completed at -196°C. Surface areas were calculated using the BET method [34]. CO adsorption isotherms obtained at 298 K using a pulse-flow method utilising an in-line gas chromatograph (Thermo Finnigan, Trace GC, TCD detector) were used to determine the chemisorption capacity of both catalysts. Assuming a surface stoichiometry of CO:Pd = 1:2 [35], these values were used to estimate Pd mean particle size. Transmission Electron Microscopy (TEM) was performed on a Tecnai T20 microscope with an accelerating voltage of 200 keV. Samples were prepared by dispersing the powder catalysts in methanol. The suspension was then dropped on a micron scale carbon grid (300 μm mesh grid, Agar scientific) and dried in a vacuum desiccator. Particle size analysis was performed with ImageJ software using the particle size routine applied to an ensemble of particles from a number of images collected from representative areas of the sample. Powder X-ray diffraction (XRD) was performed with a Siemens D5000 diffractometer (source accelerating voltage: 40 kV; source intensity: 40 mA) using $CuK_\alpha$ (1.5418 Å) radiation in Bragg-Brento geometry (range: 5-80°θ). XRD patterns were monitored using a scan rate of 0.02 ° $s^{-1}$.

### *2.2. Temperature-programmed infrared spectroscopy*

*In situ* infrared experiments were performed with a Nicolet Nexus FTIR spectrometer fitted with a SpectraTech Smart diffuse reflectance cell and environmental chamber. GU-1 was supplied as a

powder and was used directly. However, in order to obtain reasonable signal/noise IR spectra for CO chemisorption on the low loading catalyst (GU-2) it was necessary to employ a sample handling stage. Namely, scrapings of the outer layer of the catalyst pellets (diameter *ca.* 1 mm) were taken using a scalpel and placed in the sample cup of the IR cell. Isolating the outer layer of egg-shell catalysts using razors has previously been applied in TEM measurements to enhance nanoparticle numbers and permit ease of measurement [36], [37]. Thereafter, treatment of the samples was comparable for both catalysts. Reduction of the Pd nanoparticles was undertaken in a flow of He (BOC gases, 99.9%) and $H_2$ (BOC gases, 99.8%) while heating to 110°C and held at this temperature for 30 minutes. The temperature was then increased to 200°C for one hour, with $H_2$ flow stopped after 30 minutes and the sample allowed to return to ambient temperature in flowing He, where a background IR spectrum was acquired. The sample was exposed to CO (CK gases, 99.99%) and subsequently flushed with He to remove non-chemisorbed CO from the environmental chamber. Spectra were recorded at 28°C (520 scans at 4 $cm^{-1}$ resolution). For desorption experiments, the catalyst was heated *in situ* under He flow and maintained at the targeted temperature for 10 mins before cooling to 28°C for spectral acquisition. This process was repeated for 50, 100, 150, 200, 250, 300, 350, 400 and 450°C for the 5 wt % $Pd/Al_2O_3$ sample (GU-1). CO desorption temperatures up to 200°C were explored for GU-2. Due to the low metal content of this sample, the S/N ratio of the spectra were inferior to those of the higher loading sample, such that desorption measurements exceeding 200°C were uninformative. Spectra are presented as difference spectra, where the spectrum of a clean, activated catalyst has been subtracted from that of a CO dosed spectrum. No additional spectral treatment was performed.

### *2.3 Nitrobenzene hydrogenation*

Reaction testing was carried out in the vapour phase using a plug flow reactor (¼" Swagelok, internal diameter: 0.18") arrangement housed in a split tube furnace (LPC Elements). $H_2$ (25 mL $min^{-1}$) and He (12.5 mL $min^{-1}$) were supplied by mass flow controllers (Brooks, 5850 TR series). Nitrobenzene was supplied as a vapour using a heated bubbler system that delivered 0.028 μmol(nitrobenzene) $s^{-1}$. The nitrobenzene was premixed with hydrogen to a give a $H_2$ : nitrobenzene molar flow ratio of *ca.* 600:1. This large hydrogen excess was selected to expose the accessibility of all hydrogenation pathways illustrated in Scheme 2. Considering scale-up options, it is important to establish what by-products could be formed when using these $Pd/Al_2O_3$ catalysts. GU-1 was used as received, GU-2 pellets were crushed and sieved to give a powder with particle size of 500 – 250 microns. Activation of catalysts (mass ~ 27 mg) utilised a flow of $He/H_2$ (35/15 mL $min^{-1}$) and a temperature ramp (5°C $min^{-1}$) up to 200°C. The temperature was held for 1 hour with $H_2$ flow stopped after 30 minutes. All gas lines leading to and exiting the reactor were kept at a fixed temperature (60°C) using heating tape

(Electrothermal, HT95508) to ensure compounds were retained in the vapour phase. Analysis was carried out using gas-liquid chromatography via an Agilent 6850 series II fitted with a Durabond DB-17 capillary column (30 m, 0.250 mm, 0.5µm) and an FID detector. GLC samples were taken using a 250 µL gas-sampling valve. Reaction components were identified with respect to retention times of standards and quantified using response factors derived from individual calibration curves. A catalyst conditioning phase, in which the reaction was run at 60°C for 16 hours, was utilised to allow the reaction to stabilise prior to data collection. Replicate data points were collected under steady-state conditions for the following temperatures: 60, 80, 100, 120, 140, 160 and 180°C, with data presented as an average value.

Nitrobenzene conversion was calculated according to Equation 1 [38],

$$Conv.NB\ (\%) = \frac{n_{NB}(0) - n_{NB}(t)}{n_{NB}(0)} \times 100 \quad (1),$$

where $n_{NB}(0)$ represents the initial number of moles of nitrobenzene and $n_{NB}(t)$ the number of moles of nitrobenzene at time $t$. Product selectivity values were calculated according to Equation 2 [38],

$$Select.X\ (\%) = \frac{n_X(t)}{n_{total}(t) - n_{NB}(t)} \times 100 \quad (2),$$

where $n_X(t)$ represents the number of moles of compound *X* at time $t$ and $n_{total}(t)$ the total number of moles of all observed compounds at time $t$. Aniline yield values were calculated according to Equation 3 [38],

$$Yield.ANL\ (\%) = \frac{Conv.NB(t) \times Select.ANL(t)}{100} \quad (3),$$

where $Conv.NB(t)$ represents percent nitrobenzene conversion at time $t$ and $Select.ANL(t)$ the percent selectivity of aniline at time $t$. Turnover frequencies (TOF), defined as molecules reacting per second per surface metal atom [39], were calculated according to Equation 4,

$$TOF = X_{NB} \left[\frac{mol_{NB}}{mol_{Pd(s)}}\right] \quad (4),$$

where $X_{NB}$ is a fraction representing nitrobenzene conversion for a given reaction, $mol_{NB}$ represents the total number of moles of nitrobenzene per second and $mol_{Pd(s)}$ represents the number of moles of surface Pd available.

*2.4 Reaction profiles as a function of weight hourly space velocity*

Experiments assessing how the reaction profile for GU-2 was influenced by residence time were undertaken by varying the weight hourly space velocity (WHSV) at a reaction temperature of 100°C. Catalyst masses of *ca.* 25, 60, 100, 200 and 500 mg were used that respectively corresponded to WHSV values of 0.65, 0.29, 0.15, 0.08 and 0.03 $h^{-1}$. Catalyst activation and nitrobenzene hydrogenation reaction conditions, excluding reaction temperature, remained as described above.

**3. Results and Discussion**

*3.1 Catalyst characterisation*

*3.1.1 AAS, BET, CO Chemisorption and TEM*

Table 1 summarises the catalyst characterisation measurements. Palladium loadings of 4.3 ± 0.3 and 0.31 ± 0.03 wt % were observed for GU-1 and GU-2 respectively. Total surface areas for GU-1 and GU-2 were 140 ± 10 and 120 ± 8.6 $m^2 g^{-1}$. Powder XRD patterns are presented in Figure S1 and indicate the two catalysts to be based around different support materials. Whereas the reference catalyst (GU-1) used exclusively γ-alumina, the support material for the technical catalyst (GU-2) contained mixed δ and θ phases. Saturation CO values for GU-1 and GU-2 were respectively 51.0 and 3.85 μmol $g_{(cat)}^{-1}$. However, on normalisation with respect to the number of Pd atoms present, their dispersion values and, indeed, calculated mean Pd particle size are comparable (GU-1 = 4.3 ± 0.08 nm, GU-2 = 4.0 ± 0.06 nm, mean particle size 4.2 nm).

| Catalyst | Nominal Loading (wt %) | Actual Pd Loading (AAS) (wt %) | BET ($m^2$ $g^{-1}$) | Saturation coverage of CO (μmol CO $g^{-1}_{(cat)}$) | Surface Pd atoms (μmol $g_{(cat)}^{-1}$) | Catalyst Dispersion[1] (%) | Calc. Mean Pd Particle size (nm) | Observed Mean Pd Particle Size (TEM) (nm) |
|---|---|---|---|---|---|---|---|---|
| **GU-1** | 5 | 4.3 | 140 ± 10.0 | 51 ± 0.96 | 102 | 24.2 | 4.3 ± 0.08 | 5.0 ± 0.88 |
| **GU-2** | 0.3 | 0.31 | 120 ± 8.6 | 3.85 ± 0.06 | 7.69 | 27.2 | 4.0 ± 0.06 | *ca.* 5.0[2] |

Table 1. Surface area, uptake of CO, metal dispersion, particle size and concentration of surface Pd atoms for GU-1 and GU-2. TEM measured GU-1 mean Pd particle size was derived from 87

Pd crystallites. [1] Catalyst dispersion values are calculated from CO uptake. [2] Only 3 Pd crystallites were identified via TEM due to the low metal loading and poor contrast observed for this sample.

Representative transmission electron micrographs are presented in Figure 1; contrast within the images derives from both atomic number and diffractive effects, the latter making it harder to discriminate small nanoparticles from a crystalline support. Within Figure 1(a) it is possible to discern lattice spacings of the crystallites, which signify the presence of PdO ($d_{(100)}$ = 3.05 Å) and Pd metal ($d_{(111)}$ = 2.25 Å) dispersed within an amorphous alumina matrix. Figure S2 presents the particle size distribution for GU-1, which is centred about 5 nm. The low Pd loading of GU-2, and weaker contrast between the metal and support (which appears more crystalline than that of GU-1), complicated a statistically significant determination of Pd particle size for this sample, but the Pd particles were estimated to be *ca*. 5 nm in diameter. The TEM derived mean Pd particle sizes are consistent with those obtained from CO chemisorption (Table 1).

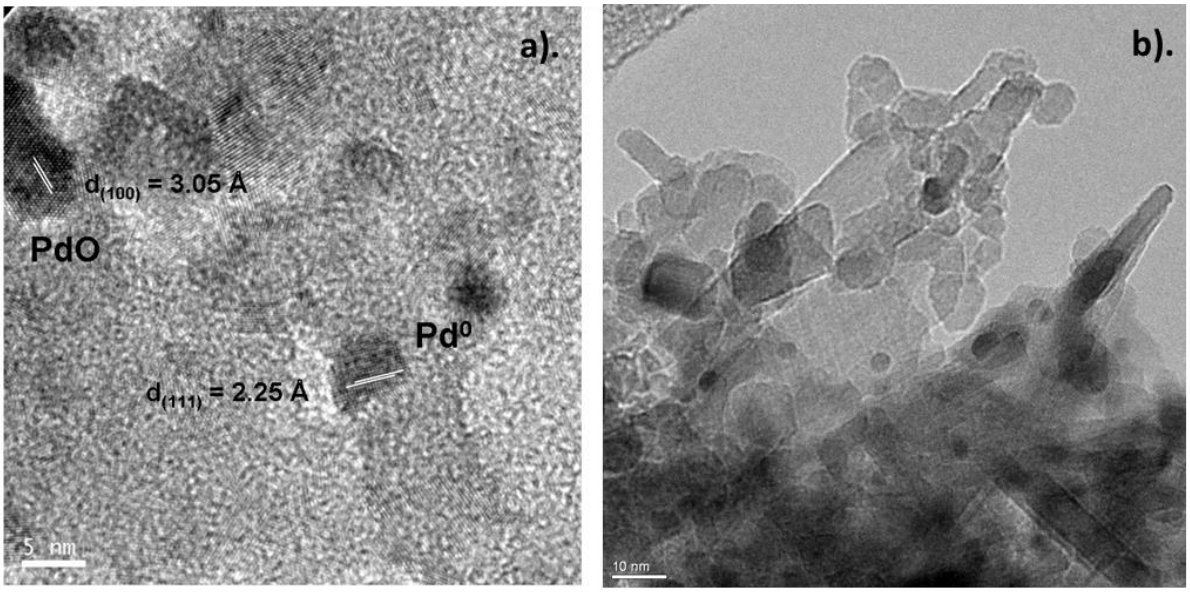


Figure 1**.** TEM micrographs: (a) GU-1 (scale bar = 5 nm), (b) GU-2 (scale bar = 10 nm). The abundance of particles from the GU-1 sample permitted an estimate of crystallite d-spacing.

### *3.1.2 CO Temperature-Programmed IR Spectroscopy*

The temperature-programmed IR spectroscopic profile for CO chemisorption over GU-1 has recently been reported over the temperature range 28-300°C [29]. Figure 2 extends this range to 450°C. The room temperature spectrum depicts 4 features: a broad band at 1903 $cm^{-1}$ assigned to $\mu_3$ bridge bonded CO on Pd(111) planes; a sharp band at 1978 $cm^{-1}$ arising from $\mu_2$ bridge bonded CO on Pd(100)

planes; and a broad feature at higher wavenumbers that can be resolved to a band at 2055 $cm^{-1}$ that is associated with linear CO adsorption to edge sites and a shoulder feature at 2077 $cm^{-1}$ arising from linear CO adsorption to corner sites [40]. The significance of distinguishing between CO adsorption on corner and edge sites, adsorption sites proposed to be involved in hydrogen supply [40], [41], [42], via DRIFTS has previously been considered [29]. Furthermore, and central to this study, is to note that the profile of the ambient temperature infrared spectrum shown in Figure 2 is indicative of the Pd crystallites adopting a truncated cubo-octahedron structure [40]. Thus, catalytic turnover on GU-1 can be considered as occurring on the Pd surface sites, as revealed within Figure 2.

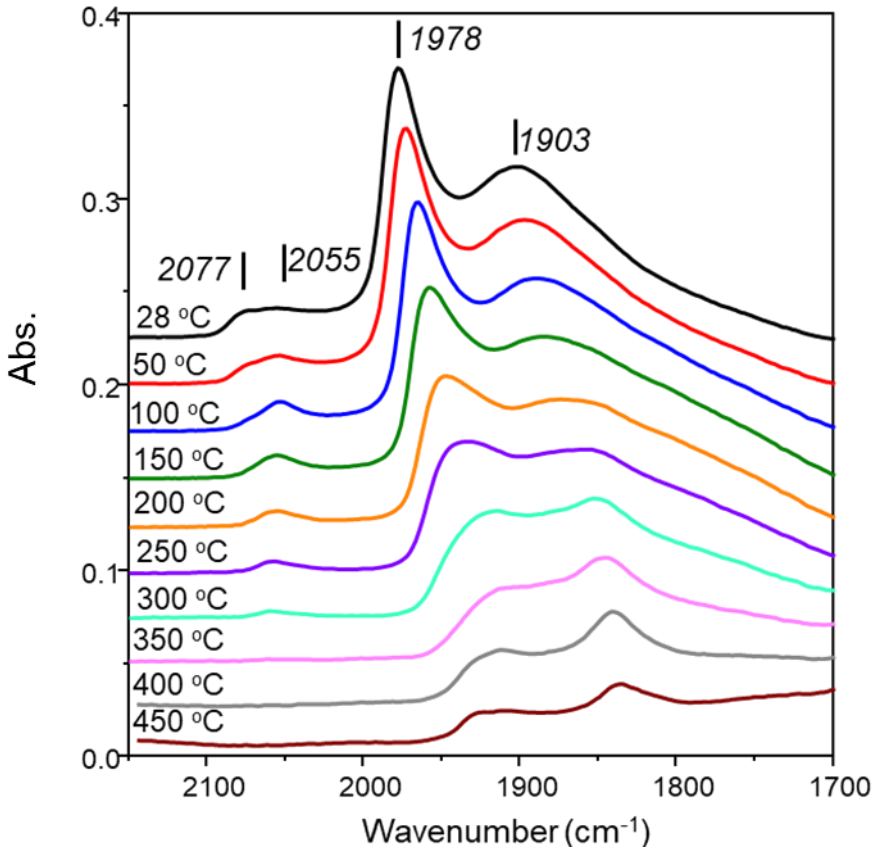


Figure 2. CO temperature-programmed IR spectra for GU-1 (28-450°C). The spectra have been offset by 0.025 au to facilitate viewing.

Figure 2 shows linearly adsorbed CO to fully desorb from GU-1 in the ranges of 50 – 100°C and 300 – 350°C for corner and edge sites, respectively; indicating the edge atoms to represent high energy sites. Bridge bonded CO was held more strongly on the catalyst and was still present in the spectrum collected after the maximum desorption temperature of 450°C. These results agree with previous CO TP-IR measurements for 5 wt % $Pd/Al_2O_3$ catalysts [29], [40], indicating GU-1 to provide a useful reference material on which to consider morphological effects on hydrogenation activity.

Figure 3 gives the CO TP-IR spectra for GU-2 recorded over the temperature range 27-200°C. As considered in Section 2.2, due to the relatively low density of surface sites (7.7 µmol $Pd_{(s)}$ $g_{(cat)}^{-1}$ *cf.* 102 µmol $Pd_{(s)}$ $g_{(cat)}^{-1}$) desorption temperatures ≥ 200°C led to insufficient $CO_{(ad)}$ to produce measurable spectra. Accepting the lower concentration of Pd in GU-2, the room temperature spectrum of Figure 3 corresponds closely to that of GU-1, with peaks observed at 2077, 2053, 1973 and 1902 $cm^{-1}$.

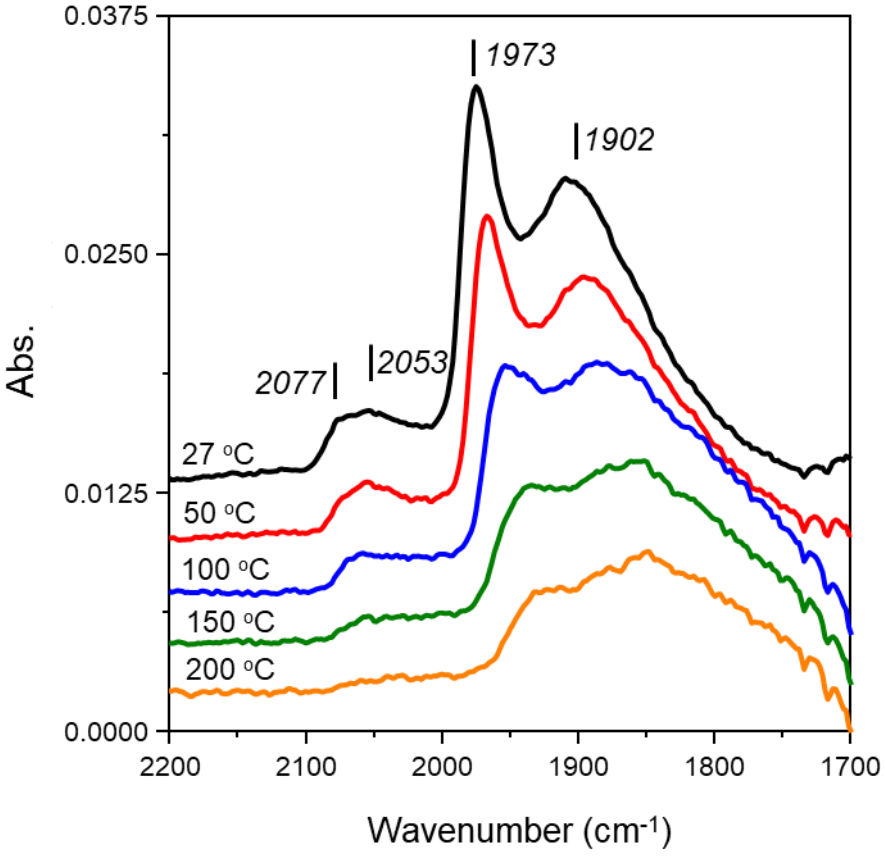


Figure 3. CO temperature-programmed IR spectra for GU-2. Note spectra have been offset by 0.025 au to facilitate viewing.

The strength of CO adsorption on GU-2 follows the trend observed with GU-1: bridge bonded CO > linear (edge) CO > linear (corner) CO. CO adsorbed linearly to corner sites desorbed in the range of 50 – 100°C and bridge bonded CO ($\mu_2$ and $\mu_3$) was present at the maximum desorption temperature of 200°C. In contrast, CO adsorbed linearly on edge sites appears to desorb in the range of 150 – 200°C, a significant reduction compared to GU-1 (300 – 350°C). It is possible that this difference in spectral profiles merely reflects the lower spectral intensity encountered with the lower loading sample. Importantly, on comparing Figure 3 with Figure 2, GU-2 is seen to possess a similar profile to that encountered with GU-1, indicating the morphology of the particles of the industrial grade, low Pd loading variant to be comparable to the reference catalyst. Moreover, as Section 3.1.1 shows both

samples to possess comparable mean Pd particle size (~5 nm), GU-1 can be used to infer insight on the morphological trends connected with hydrogenation activity of the industrial specification $Pd/Al_2O_3$ catalyst (GU-2).

### *3.2 Reaction Testing*

Figure 4 shows near complete nitrobenzene conversion was achieved with both catalysts throughout the temperature range studied: GU-1 ≥ 99.92%; GU-2 ≥ 99.96%. This was facilitated by the elevated temperatures and large excesses of hydrogen used ($H_2$:NB = *ca.* 600:1). Each catalyst data set corresponds to a different turnover frequency (TOF): $TOF_{(GU-1)}$ = 0.01 $s^{-1}$; $TOF_{(GU-2)}$ = 0.13 $s^{-1}$. TOF is determined with respect to the nitrobenzene conversion, the number of moles of nitrobenzene and the number of moles of surface Pd [39]. As nitrobenzene flow was fixed and nitrobenzene conversion was near complete for both data sets, variances in TOF reflect the different metal loadings associated with GU-1 and GU-2. Operation at full nitrobenzene conversion is representative of the industrial scenario [3]. Comparison of aniline selectivity for both data sets (Figure 4) showed a decrease with increasing reaction temperature for both GU-1 and GU-2, however, the exact aniline selectivity values varied. A maximum of 88% aniline selectivity was observed for GU-1, which decreased to 35% as reaction temperatures were elevated to 180°C. In contrast, GU-2 exhibited an initial aniline selectivity of 97% at 60°C that decreased to 68% with increasing temperature. Thus, the lower Pd weighting catalyst (GU-2) shows greater aniline selectivity than GU-1 under the stated conditions. Blank reaction testing on a reference γ-alumina sample revealed minimal nitrobenzene conversion, therefore it is deduced that all the hydrogenation activity is attributed to the presence of the Pd nanoparticles for GU-1. The authors were unable to obtain a source of the mixed phase alumina associated with the technical catalyst (GU-2), therefore a probable role for the support in the chemistry facilitated over this material is unknown.

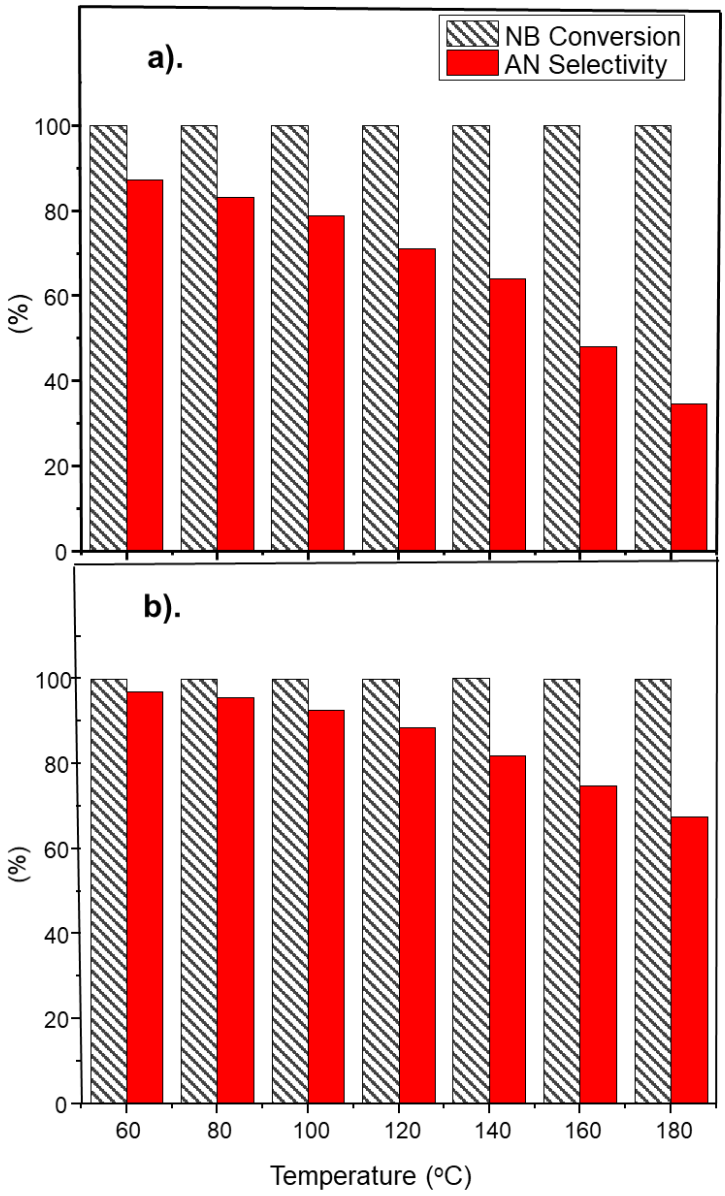


Figure 4. Nitrobenzene conversion (grey hatched columns) and aniline selectivity (red columns) as a function of temperature recorded at a WHSV of 0.46 $h^{-1}$: (a) GU-1; (b) GU-2. Temperature ramping was initiated after a 16 hr reaction conditioning phase undertaken at 60°C.

Consideration of the distribution of by-products observed during hydrogenation is critical for determining variations in catalytic activity and for product purification on scale-up. By-products detected during testing of GU-1 and GU-2 revealed that the dominant cause for loss of aniline selectivity in both cases was owed to the over-hydrogenation of aniline. Over-hydrogenation of aniline during nitrobenzene hydrogenation is well documented [21], [22], [43] and is reported to arise via an amine intermediate that is either hydrogenated to give cyclohexylamine (CHA) or coupled with

aniline to give a phenylamine intermediate, which then undergoes subsequent hydrogenation to N-cyclohexylaniline (CHAN) and finally dicyclohexylamine (DICHA) [21].

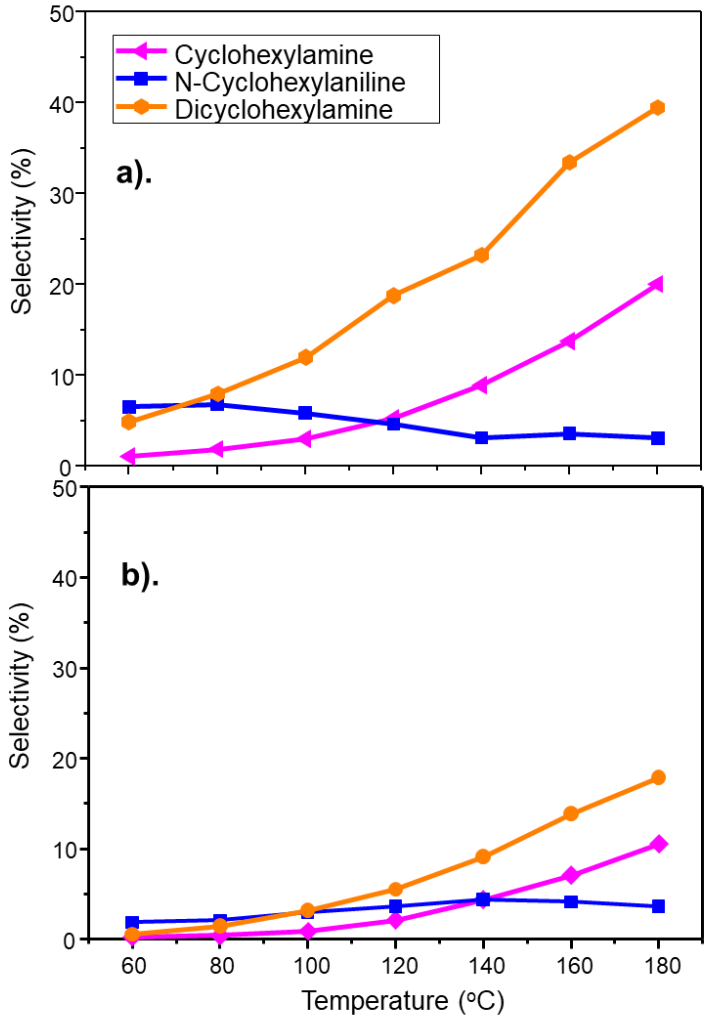


Figure 5. Selectivity of aniline over-hydrogenation by-products [Pathway-1] CHA (pink), CHAN (blue) and DICHA (orange) as a function of increasing temperature at a WHSV of 0.46 $h^{-1}$: (a) GU-1; (b) GU-2. Temperature ramping was initiated after a 16 hr reaction conditioning phase undertaken at 60°C.

Selectivities to the by-products derived from aniline hydrogenation are presented in Figure 5. Reflecting the trends observed in Figure 4, the extent of aniline hydrogenation by-product formation is significantly greater for GU-1 but, nevertheless, comparable trends are observed for both catalysts: namely, [DICHA] > [CHA] > [CHAN]. This reproducibility of trends for both catalysts is suggestive of a stepwise hydrogenation pathway as illustrated in Scheme 3.

NB → AN → CHA → CHAN → DICHA

Scheme 3. Proposed stepwise hydrogenation pathway for aniline derived by-products.

Clearly, GU-1 facilitates aniline hydrogenation to a greater extent than observed for GU-2. As GU-1 and GU-2 have similar Pd particle sizes (Section 3.1.1) and distribution of Pd sites (Section 3.1.2), the loss of aniline selectivity associated with GU-1 compared to GU-2 can be assigned to the presence of a higher quantity of Pd crystallites and, importantly, not any structural difference between the two catalysts. Whereas Figure 5 shows DICHA to be the major product, this outcome differs from the liquid phase reaction results reported by Sá Couto and co-workers, who report higher levels of CHA and CHAN than DICHA [21]. It is possible that this difference in product selectivity is attributable to differences in Pd crystallite morphology or, alternatively, reflects mass transfer issues associated with the liquid phase reaction.

Figure 6 shows further by-products are observed, which are classified as nitrobenzene-derived intermediates, cyclohexanone (CHO) and cyclohexanol (CHOL), with CHOL being a hydrogenation product of CHO [21]. Additionally, at temperatures < 160°C an unknown species is detected for GU-2 (Fig.6(b)). As its retention time is very close to that of CHO, it is thought to be an intermediate between a nitrobenzene derived surface species and CHO. Work is underway to identify this molecule, whose GC retention time does not correspond to any obvious candidate. Products (CHO and CHOL) derived from this route are referred to as Pathway 2 by-products (Scheme 2, green).

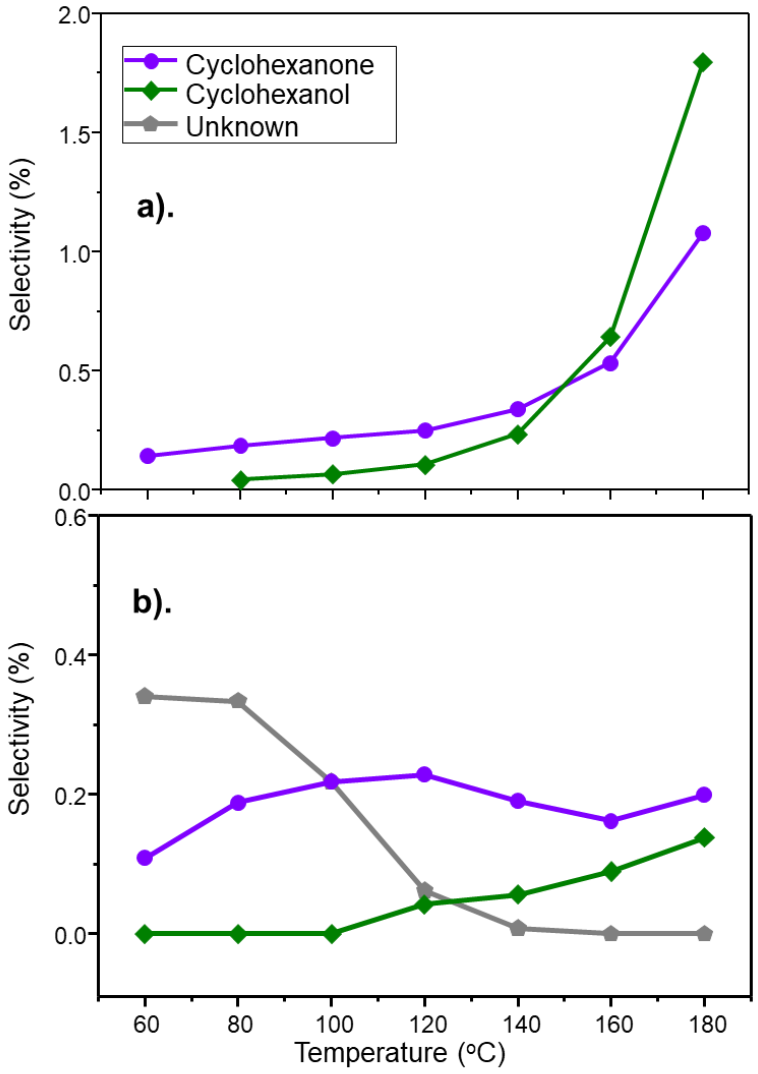


Figure 6. Selectivity of by-products derived from nitrobenzene intermediates CHO (purple) and CHOL (green) as a function of increasing temperature at a WHSV of 0.46 $h^{-1}$: (a) GU-1; (b) GU-2. Temperature ramping was initiated after a 16 hr reaction conditioning phase undertaken at 60°C. An unknown by-product was uniquely detected with GU-2. This moiety is indicated by grey pentagons, with the concentration estimated using the CHO GC response factor.

The extent of Pathway 2 by-products is much less than observed for Pathway 1. A maximum selectivity for a Pathway 1 derived by-product of *ca.* 40% (DICHA, Fig. 5(a)) was observed for GU-1. Comparatively, the maximum selectivity observed for Pathway 2 derived by-products for GU-1 was *ca.* 1.8% and owed to CHOL production (Fig. 6(a)). This dramatic variation in by-product distributions between the 2 pathways investigated here cements the nature of the $Pd/Al_2O_3$ catalysts to favour hydrogenation reactions over other transformations (*e.g.*, coupling reactions involving nitrobenzene

derived intermediates [21]), and highlights the relevance, and indeed requirement, of characterising catalyst sites involved in hydrogen supply. As considered previously, Pd edge and corner sites are thought to play an important role in maintaining hydrogen supply [29]. With reference to Figure 2 that shows edge sites to exhibit the higher enthalpy of adsorption of the terminal sites, it is tentatively suggested that these sites are active in facilitating dissociative adsorption of dihydrogen [29] that, subsequently, participates in surface-mediated hydrogenation reactions.

A combination of Figures 4, 5 and 6 indicate that although the extent of by-product formation is greater with GU-1, nevertheless, GU-2 displays comparable profiles involving the same chemical entities. This comparison demonstrates that comparable surface chemistry is observable in each case with Figure 3 indicating that GU-2 possesses a similar active site distribution to that observed for the reference catalyst GU-1 (Figure 2). Thus, it is the higher concentration of ~5 nm Pd crystallites of GU-1 that is responsible for the greater degree of by-product formation. Finally for this section, it is additionally noted that the difference in support materials for the two catalysts (Section 3.1.1) appears not to have unduly influenced the product distributions observed, confirming the surface chemistry evident in Figures 4,5 and 6 to be Pd-mediated.

### *3.3 GU-2: Weight Hourly Space Velocity dependence*

Section 3.2 showed the technical catalyst GU-2 to exhibit superior aniline selectivity compared to the reference catalyst. Therefore, this catalyst was scrutinised further by examining reaction profiles at an elevated temperature as the weight hourly space velocity was varied in the range of 0.65-0.03 $h^{-1}$. A reaction temperature of 100°C was selected for these WHSV studies, which provide insight on whether extended contact with the catalyst can affect catalytic performance. Section 3.2 indicated over-hydrogenation of aniline to be the primary cause of selectivity loss, thus reaction testing for WHSV focused on these downstream products (Scheme 2, Pathway 1).

Figure 7 presents nitrobenzene conversion as a function of time-on-stream for 5 WHSV values: 0.65, 0.29, 0.15, 0.08 and 0.03 $h^{-1}$. For WHSV values $\leq$ 0.15 $h^{-1}$ complete nitrobenzene conversion was observed, whereas for WHSV values $\geq$ 0.29 $h^{-1}$ only partial conversion was achieved. In the case of WHSV = 0.29 $h^{-1}$, conversion was reasonably constant throughout the 700 min reaction period studied: initial nitrobenzene conversion = 89%; final conversion = 84%. In contrast, the WHSV of 0.65 $h^{-1}$ showed a decline in nitrobenzene conversion from an initial value of 81% to a final value of 63%. Thus, it appears that a catalyst deactivation channel is evident on operation at higher space velocities. Figure 7 also indicates that a minimum residence time is required to ensure full nitrobenzene

conversion. This is because the relatively low Pd loading of GU-2 means that short residence times with this material leads to insufficient contact with surface Pd atoms to effect full conversion. However, for a fixed feedstock flow rate, extending catalyst mass increases the exposure to $Pd_{(s)}$, thereby increasing nitrobenzene consumption.

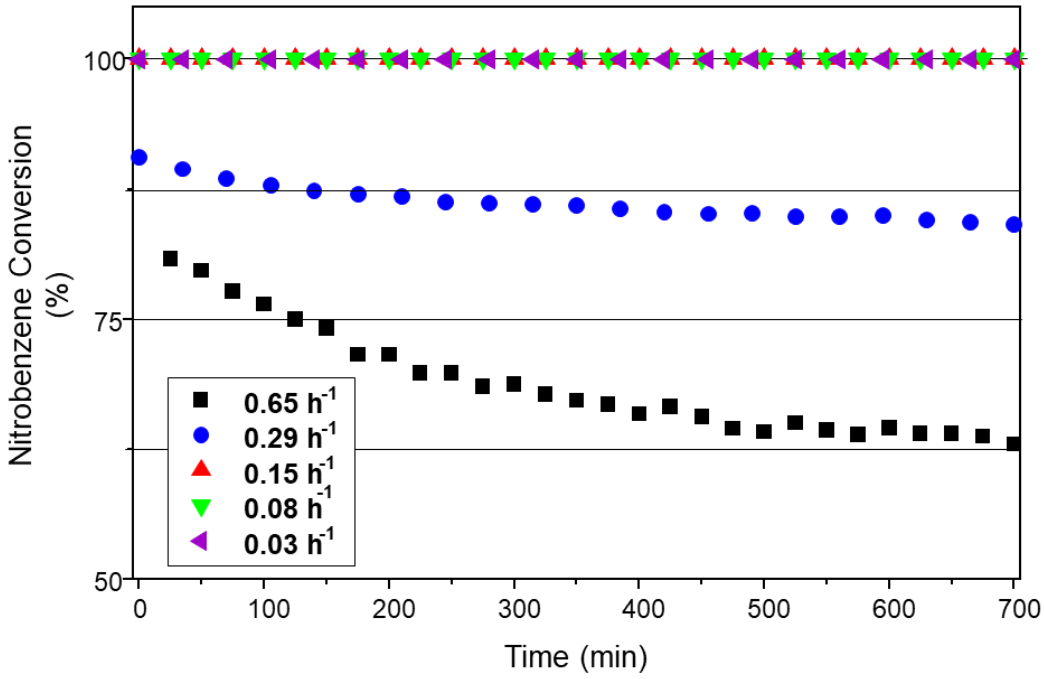


Figure 7. Nitrobenzene conversion for GU-2 as a function of time-on-stream and operation at different WHSV values: 0.65 (black), 0.29 (blue), 0.15 (red), 0.08 (green) and 0.03 (purple) $h^{-1}$. Reaction temperature: 100°C; feed ratio, $H_2$:NB = 600:1; incident nitrobenzene flux = 0.028 μmol(nitrobenzene) $s^{-1}$; total gas flow 37.5 ml $min^{-1}$.

Figure 8 shows the corresponding aniline selectivity values as a function of time-on-stream as WHSV's are varied and reveals some distinct trends. Selectivity for a WHSV of 0.65 $h^{-1}$ showed an initial dip to *ca.* 87%, however after ~300 minutes run time selectivity recovered and settled at 99%. This was the only WHSV value to show an increase in aniline selectivity with increasing run time. WHSV values of 0.29 and 0.15 $h^{-1}$ exhibited similarly high aniline selectivities of *ca.* 98 and 97%, respectively, at steady-state. Significant declines in aniline selectivity were observed for WHSV's of 0.08 and 0.03 $h^{-1}$, with respective steady-state selectivities of 90 and 79% observed. This trend is indicative of a catalyst conditioning phase during the initial ~100 minutes of the reaction. In this way, Figures 7 and 8 are indicating a degree of complexity within the reaction system, which the authors attribute to the dynamics of the hydrogenation process. Specifically, for a fixed incident hydrogen/nitrobenzene feed over GU-2, with an excess of hydrogen relative to hydrocarbon, catalyst masses equal to and

exceeding 200 mg (WHSV: ≤ 0.08 $h^{-1}$) signify the stage at which the surface hydrogen supply (via dissociative adsorption of dihydrogen) exceeds the nitrobenzene adsorption rate and, consequently, leads to the formation of higher hydrogenated products that compromise product selectivity. Thus, Figure 8 indicates that in the presence of a large hydrogen excess over a low loading technical grade catalyst that WHSV is an operational parameter. Equally, this analysis additionally signifies that incident hydrogen concentrations could also be adjusted to reduce the probability of the occurrence of over-hydrogenation reactions.

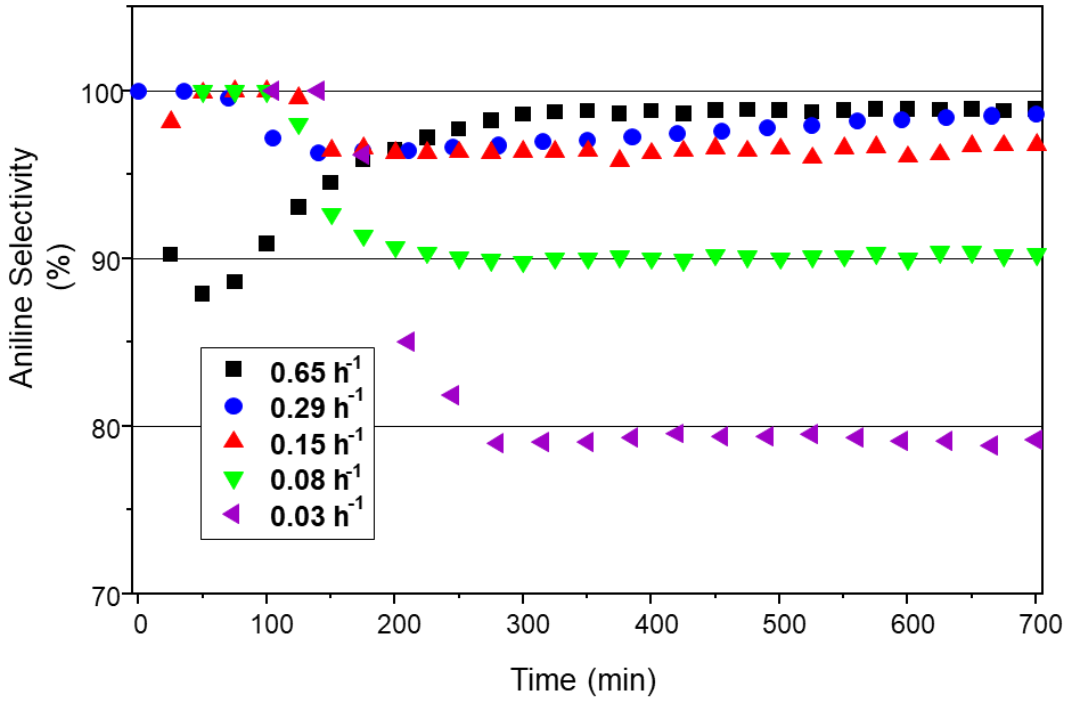


Figure 8. Aniline selectivity for GU-2 as a function of time-on-stream and operation at different WHSV values: 0.65 (black), 0.29 (blue), 0.15 (red), 0.08 (green) and 0.03 (purple) $h^{-1}$. Reaction temperature: 100°C; feed ratio, $H_2$:NB = 600:1; incident nitrobenzene flux = 0.028 μmol(nitrobenzene) $s^{-1}$; total gas flow 37.5 ml $min^{-1}$.

Figure 9 complements Figure 8 by presenting a profile of how the by-products are distributed as a function of WHSV. For the fixed (excess) hydrogen flow rate considered in this study, increased quantities of Pd in the reactor results in increased formation of aniline over-hydrogenation by-products. As the WHSV decreases (increasing catalyst mass), Figure 9 shows that the extent of DICHA formation increases. This observation is consistent with the proposal outlined in Scheme 3, in which DICHA is the final product in a consecutive hydrogenation pathway. It is interesting to note that the extent of CHAN formation appears to be insensitive to WHSV. This outcome may be rationalised with

reference to Scheme 3, with CHAN being an intermediate between CHA and DICHA and it is the interplay between the concentration of CHA and the rapid hydrogenation of CHAN to DICHA that sustains the CHAN concentration at an approximately constant level within a consecutive reaction sequence. Sá Couto et al. invoke a different route for CHA formation (Scheme 2) [21]. Work is underway to further evaluate the validity of Scheme 3.

At the highest WHSV of 0.65 $h^{-1}$ Figure 9 reveals the presence of a small quantity of azobenzene (AZO) alongside a larger component of CHAN. The AZO is thought to be derived from the coupling of nitrobenzene derived intermediates nitrosobenzene and phenylhydroxylamine, which is indicative of an incomplete pathway in aniline formation [13], [14]. This was the only occasion when potentially hazardous azo compounds were encountered over the two catalysts studied. Figure 9 indicates such processes to be inherently disfavoured over GU-2, although possible to a limited degree at high space velocities where hydrogenation pathways are less favoured.

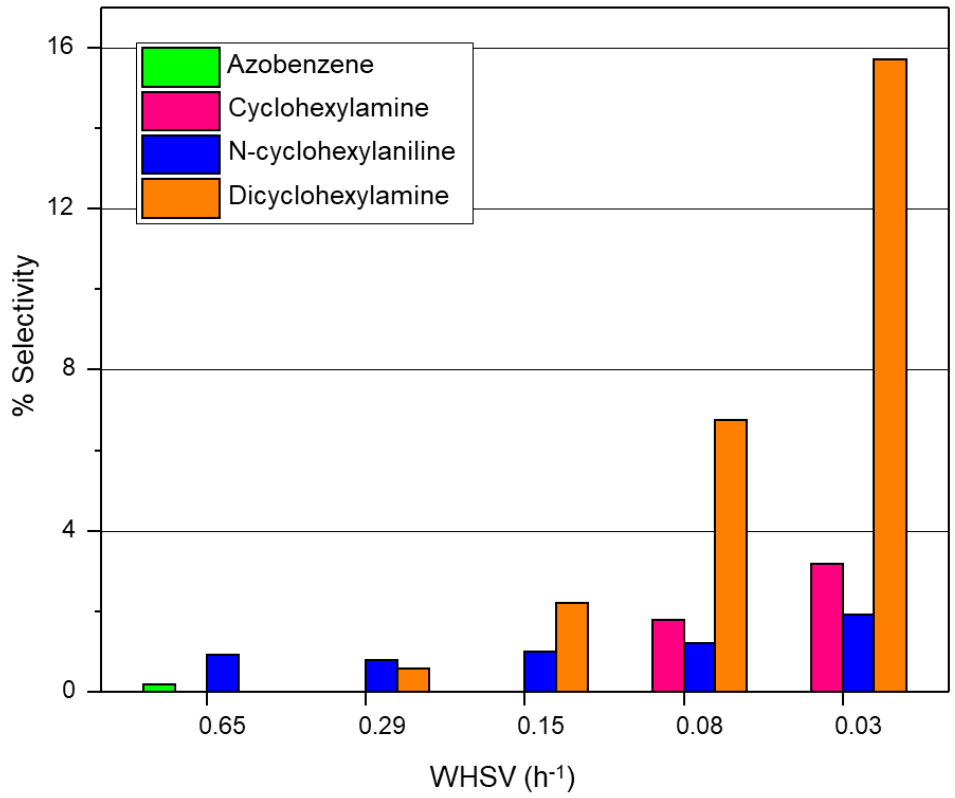


Figure 9. Plot of GU-2 by-product selectivity at steady-state operation as a function of WHSV. Reaction temperature: 100°C; feed ratio, $H_2$:NB = 600:1; incident nitrobenzene flux = 0.034 µmol(nitrobenzene) $s^{-1}$; total gas flow 37.5 ml $min^{-1}$. Pathway 2 derived products CHO and CHOL (Scheme 2, green) are not included in this plot but were present in quantities < 0.2%.

Figure 10 provides a plot of aniline yield as a function of WHSV under steady-state conditions over GU-2 at 100°C and shows that a WHSV of 0.15 $h^{-1}$ (catalyst mass 100 mg) provides the optimal conditions for a maximised aniline yield of 97% within the stated configuration. This outcome is close to industrial performance specifications [3].

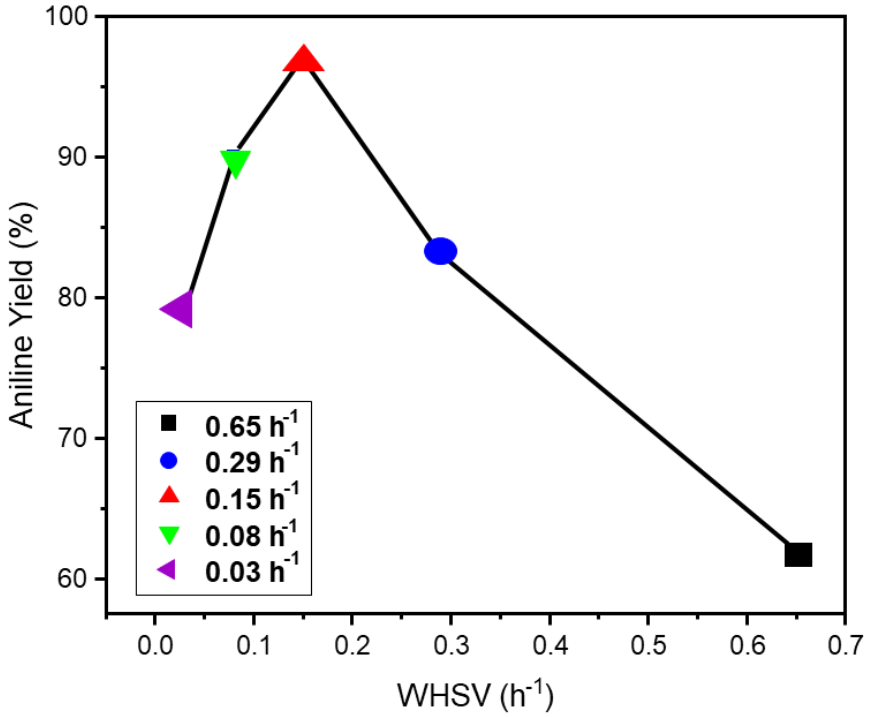


Figure 10. Plot of aniline yield as a function of increasing WHSV for GU-2. Reaction temperature: 100°C; feed ratio, $H_2$:NB = 600:1; incident nitrobenzene flux = 0.034 µmol(nitrobenzene) $s^{-1}$; total gas flow 37.5 ml $min^{-1}$.

Bringing these outcomes together, for a defined Pd crystallite morphology (as defined by Figures 2 and 3) operating within a fixed nitrobenzene feed rate and excess hydrogen, relatively high Pd loadings will lead to a loss of aniline selectivity due to over-hydrogenation of predominantly aniline derived products. As indicated in Figure 10, a matching of catalyst contact times can mitigate product loss for the low loading industrially relevant catalyst specification. The catalysts can be operated to avoid the formation of nitrobenzene derived coupling products, which simplifies purification requirements for reactor exit streams. Future work will examine further how Pd particle morphology may be more explicitly linked to sustained aniline yields. A correlation between catalyst specification and by-product formation during operation at elevated temperatures are prerequisite design inputs for energy efficient large-scale aniline synthesis plants.

## 4. Conclusions

Two $Pd/Al_2O_3$ catalysts (GU-1 and GU-2) have been examined for their suitability as aniline synthesis catalysts for application in a unit operation with suitable heat recovery capability. Nitrobenzene hydrogenation in the vapour phase has been investigated in a microreactor arrangement in the presence of a large hydrogen excess. These conditions were selected to expose the hydrogenation pathways accessible with these catalysts. The following conclusions can be drawn.

- GU-1 and GU-2 possess comparable Pd particle sizes of ~ 5 nm. Comparisons with GU-1 as a reference catalyst, combined CO chemisorption and TPIR spectroscopic measurements, indicate Pd nanoparticles of the low Pd loading technical catalyst to approximate to truncated cubo-octahedra.
- Reaction testing over the temperature range 60-180°C shows the smaller concentration of Pd crystallites of GU-2 significantly reduces over-hydrogenation of aniline, a major cause for loss of product selectivity.
- Although the extent of by-product formation is greater with GU-1, nevertheless, GU-2 displays comparable profiles involving the same chemical entities. This indicates that comparable surface chemistry is observable in each case and is consistent with the deduction that GU-2 possesses a similar active site distribution to that observed for the reference catalyst (GU-1).
- The presence of two major by-product formation pathways is confirmed: Pathway-1, the direct over-hydrogenation of aniline; Pathway-2, the transformation of nitrobenzene to cyclohexanone, which can then be further hydrogenated to cyclohexanol. Pathway-1 dominates and is thought to represent a consecutive hydrogen addition process.
- For GU-2 at 100°C and WHSV values $\leq 0.08\ h^{-1}$ aniline selectivity is compromised via product over reduction.
- A plot of aniline yield versus WHSV for GU-2 at 100°C yields a 'volcano' type curve that peaks at an aniline selectivity of 97% at a WHSV value of $0.15\ h^{-1}$.
- There is evidence of a catalyst conditioning period that affects aniline selectivity.

**Supporting Information**

Figure S1: XRD diffraction patterns for GU-1 and GU-2; Figure S2: TEM derived particle size distribution of Pd crystallites for GU-1.

**Acknowledgements**

The College of Science and Engineering (GU), the School of Chemistry (GU), Huntsman Polyurethanes and the EPSRC are thanked for project support and the provision of Ph.D. studentships (CGAM, JWC,

AMM [EP/R513222/1 & EP/N509668/1]). Dr Don Jones (Huntsman Polyurethanes) is thanked for helpful discussions.

## References

[1] Brereton, G. Polyurethanes. In *Ullmann's Encyclopedia of Industrial Chemistry*; Ley, C., Elvers, B., Eds.; Wiley: Weinheim, 2019**;** pp 1-76.

[2] Six, C.; Richter, F. Isocyanates, Organic. In *Ullmann's Encyclopedia of Industrial Chemistry*; Ley, C., Elvers, B., Eds.; Wiley: Weinheim, 2012**;** pp 63-82.

[3] Kahl, T.; Schröder, K. W.; Lawrence, F.; Marshall, W.; Höke, H.; Jäckh, R. Aniline. In *Ullmann's Encyclopedia of Industrial Chemistry*; Ley, C., Elvers, B., Eds.; Wiley: Weinheim, 2012; pp 45-478.

[4] Randall, D.; Lee, S. *The Polyurethanes Book*; John Wiley & Sons: New York, 2002.

[5] Elsido, C.; Martelli, E.; Kreutz, T. Heat integrations and heat recovery steam cycle optimisation for a low carbon lignite/biomass-to-jet fuel demonstration project. *Appl. Energy* **2019**, *239*, 1322 - 1342, DOI: 10.1016/j.apenergy.2019.01.221

[6] Li, M.; Zhuang, Y.; Zhang, L.; Lui, L.; Du, J.; Shen, S. Conceptual design and techno-economic analysis for a coal-to-SNG/methanol polygeneration process ins eries and parallel reactors with intergration of waste heat recovery. *Energy Convers. Manag.* **2020***, 214*, 112890, DOI:10.1016/j.enconman.2020.112890

[7] Huang, B.; Li, Y.; Gao, R.; Zuo, Y.; Dai, Z.; Wang, F. Simultaneous optimisation and heat integration of the coal-to-SNG process with a branched heat recovery steam cycle. *Comput. Chem. Eng.* **2018***, 117*, 117-128, DOI: 10.1016/j.compchemeng.2018.02.008

[8] Bianco, N.; Fragnito, A.; Iasiello, M.; Mauro, G. An inexpensive approach for the multi-objective optimisation of heat recovery steam generation to maximise cost effectiveness and output power. *Sustain. Energy Technol.* **2021***, 45*, 101162, DOI: 10.1016/j.seta.2021.101162.

[9] Barker, G. *The engineer's guide to plant layout and piping design for oil and gas industries*; Gulf Professional Publishing: Oxford, 2018.

[10] Law, C.; Chen, H.; Mujumdar, A. Food Technologies: Drying. *Encyclopedia of Food Safety*. **2014**, *3,* 156-167, DOI:10.1016/B978-0-12-378612-8.00268-7

[11] Vakkilainen, E. *Steam Generation from Biomass*: Butterworth-Heinmann, 2017.

[12] NIST Chemistry WebBook. *NIST Standard Reference Database Number 69.* NIST, 2021. DOI: https://doi.org/10.18434/T4D303. (accessed 2021-11-02).

[13] Haber, F.; Über stufenweise redukton des nitrobenzols mit begrenztem kathodenpotential. *Z. Elektrochem. Angew. Phys. Chem.* **1898***, 4*, 506.

[14] Gelder, E.; Jackson, S. D.; Lok, C. M.; The hydrogenation of nitrobenzene to aniline: a new mechanism. *Chem. Comm.* **2005***, 4*, 522 - 524, DOI:10.1039/B411603H

[15] Relvas, J.; Andrade, R.; Friere, F.; Lemos, F.; Araújo, P.; Pinho, M.; Nunes, C.; Ribeiro, F. Liqid phase hydrogenation of nitrobenzene over an industrial Ni/SiO2 supported catalyst. *Catal. Today* **2008***, 133*, 828 - 835, DOI:10.1016/j.cattod.2007.11.050

[16] Zhao, F.; Ikushima, Y.; Arai, M. Hydrogenation of nitrobenzene with supported platinum catalysts in supercritical carbon dioxide: effect of pressure, solvent and metal particle size. *J. Catal.* **2004***, 224*, 479 - 483, DOI:10.1016/j.jcat.2004.01.003

[17] Diao, S.; Qian, W.; Luo, G.; Wei, F.; Wang, Y. Gaseous catalytic hydrogenation of nitrobenzene to aniline in a two-stage fluidized bed reactor. *Appl. Cat. A: Gen.* **2005***, 286*, 30 - 35, DOI:10.1016/j.apcata.2005.02.026

[18] Turáková, M.; Salmi, T.; Eränen, K.; Wärna, J.; Murzin, D. Y.; Králik, M. Liquid phase hydrogenation of nitrobenzene, *Appl. Cat. A: Gen.* **2015***, 499*, 66 - 76, DOI:10.1016/j.apcata.2015.04.002

[19] Qu, Y.; Chen, T;. Wang, G. Hydrogenation of nitrobenzene catalysed by Pd promoted Ni supported on C60 derivative. *Appl. Surf. Sci.* **2019***, 465*, 888-894, DOI: 10.1016/j.apsusc.2018.08.199

[20] Simescu-Lazar, F.; Meille, V.; Bornette, F.; Campoli, F.; de Bellefon, C. In situ electrochemical regeneration of deactivated coated foam catalysts in a Robinson-Mahoney basket reactor: Example of Pd/C for nitrobenzene hydrogenation. *Catal. Today* **2015***, 249*, 52 - 58, DOI:10.1016/j.cattod.2014.12.046

[21] Sá Couto, C.; Maderia, L.; Nunes, C. P.; Araujo, P. Hydrogenation of nitrobenzene over a Pd/Al2O3 catalyst - Mechanism and effect of the main operating conditions. *Chem. Eng. Tech.* **2015***, 38*, 1625 - 1636, DOI: 10.1002/ceat.201400468

[22] Sá Couto, C.; Maderia, L.; Nunes, C. P.; Araujo, P. Commercial catalysts screening for nitrobenzene hydrogenation. *Appl. Cat. A: Gen.* **2016***, 522*, 152 - 164, DOI:10.1016/j.apcata.2016.04.032

[23] Sá Couto, C.; Maderia, L.; Nunes, C. P.; Araujo, P. Liquid-phase hydrogenation of nitrobenzene in a tubular reactor: parametric study of operation conditions influence. *Ind. Eng. Chem. Res.* **2017***, 56*, 3231 - 3242, DOI:10.1021/acs.iecr.7b00403

[24] Zhang, L.; Zhou, M.; Wang, A.; Zhang, T. Selective hydrogenation over supported metal catalysts: From nanoparticles to single atoms. *Chem. Rev.* **2020***, 120*, 683 - 733, DOI: 10.1021/acs.chemrev.9b00230

[25] Zhang, X.; Gu, Q.; Ma, Y.; Guan, Q.; Jin, R.; Wang, H.; Yang,B.; Lu, J. Support-induced unusual size dependence of Pd catalysts in chemoselective hydrogenation of para-chloronitrobenzene. *J. Catal.* **2021***, 400*, 173 - 183, DOI: 10.1016/j.jcat.2021.06.002

[26] Murata, K.; Shiotani, T.; Ohyama, J.; Satsuma, A. Selective hydrogenation of C=C bond in cinnamaldehyde on Pd set sites of $Pd/Al_2O_3$. *Chem. Lett.* **2021***, 50*, 599 - 602, DOI:10.1246/cl.200856

[27] Mitchell, C. J.; Stewart, D. Process for the conversion of aromatic nitro compound into amines. U.S. Patent WO 2011/113491; 2011.

[28] Päßler, F.; Freund, H-J. Model-based design of energy efficient reactors. *Chem. Ing. Tech.* **2018***, 90*, 852 - 863, DOI:10.1002/cite.201700124

[29] McCullagh, A. M.; Warringham, R.; Morisse, C. G. A.; Gilpin, L.; Brennan, C.; Mitchell, C. J.; Lennon, D. A comparison of experimental procedures for the application of infrared spectroscopy to probe the surface morphology of an alumina supported palladium catalyst. *Top. Catal.* **2021***,* 1-11*,* DOI: 10.1007/s11244-021-01435-y

[30] Satterifeld, C. N. *Heterogeneous Catalysis in Industrial Practice, 2nd Edition;* Krieger Publishing Company: Florida, 1991.

[31] Bartholomew, C. H.; Farrauto, R. J. *Fundamentals of Industrial Catalytic Processes*; John Wiley & Sons, INC.: New Jersey, 2006.

[32] Ché, M.; Clause, O.; Marcilly, C. H. Impregnation and Ion Exchange. In *Handbook of Heterogeneous Catalysis, Vol. 1*; Ertl, G., Knözinger, H., Weitkamp, J., Eds.; Wiley-VCH: Weinheim, 1997; pp 191-207.

[33] Vimont, A.; Thibault-Starzyk, F.; Daturi, M. Analysing and understanding the active site by IR spectroscopy. *Chem. Soc. Rev.* **2010***, 39*, 4928 - 4950, DOI: 10.1039/B919543M

[34] Banauer, S.; Emmet, P. H.; Teller, E. Adsorption of gases in multimolecular layers. *J. Am. Chem. Soc.* **1938***, 60*, 309 - 319, DOI:10.1021/ja01269a023

[35] Lennon, D.; Marshall, R.; Webb, G.; Jackson, S. D. The effect of hydrogen concentration on propyne hydrogenation over a carbon supported palladium catalyst studied under continuous flow conditions. *Stud. Surf. Sci. Catal.* **2000***, 130*, 245, DOI:10.1016/S0167-2991(00)80964-7

[36] Liu, R. J.; Crozier, P. A.; Smith, C. M.; Hucul, D. A.; Blackson, J.; Salaita, G. In Situ electron microscopy studies of the sintering of palladium nanoparticles on alumina during catalyst

regeneration processes. *Microscopy and Microanalysis* **2004***, 10*, 77-85, DOI: 10.1017/S1431927604040188

[37] Vita, A.; Italiano, C.; Ashraf, M. A.; Pino, L.; Specchia, S. Syngas production by steam and oxy-steam reforming of biogas on monolith-supported CeO2-based catalysts. *Int. J. Hydrogen Energy* **2018***, 43*, 11731-11744, DOI: 10.1016/j.ijhydene.2017.11.140

[38] Weissermal, K.; Arpe, H-J. *Industrial Organic Chemistry, Fourth Completely Revised Edition; Wiley*, Heppenheim, 2003.

[39] Boudart, M. Heterogeneous catalysis by metals. *J. Mol. Cat.* **1985***, 30*, 27-38, DOI:10.1016/0304-5102(85)80014-6

[40] Lear, T.; Marshall, R.; Lopez-Sanchez, J. A.; Jackson, S. D.; Klapötke, T. M.; Bäumer, M.; Rupprechter, G.; Freund, H. J.; Lennon, D. The application of infrared spectroscopy to probe the surface morphology of alumina-supported palladium catalysts. *J. Chem. Phys.* **2005***, 123*, 174706, DOI: 10.1063/1.2101487

[41] Primet, M.; Basset, J. M.; Mathieu, M. V. Infrared determination of the isotherm of hydrogen adsoprtion on a Pt/Al2O3 catalyst. *J. Chem. Soc. Faraday Trans. 1* **1974***, 70*, 293-298, DOI:10.1039/F19747000293

[42] Morkel, M.; Rupprechter, G.; Freund, H. J. Finite size effects on supported Pd nanoparticles: Interaction of hydrogen with CO and C2H4. *Surf. Sci.* **2005***, 588*, 209-219, DOI:10.1016/j.susc.2005.05.037

[43] Pikna, L. ; Heželová, M. ; Demčáková, S. ; Smrčová, M. ; Plešingerová, B. ; Štefanko, M. ; Turáková, M. ; Králik, M. ; Puliš, P. ; Lehocký, P. Effect of support on activity of palladium catalysts in nitrobenzene hydrogenation. *Chem. Pap.* **2013** *, 68*, 591 - 598, DOI:10.2478/s11696-013-0497-3

For Table of Contents only